Published for SISSA by Springer

Received: June 18, 2024
Revised: July 26, 2024
Accepted: August 21, 2024
Published: September 16, 2024

The distribution amplitude of the η_c-meson at leading twist from lattice QCD

B. Blossier,[a] **M. Mangin-Brinet**,[b] **J.M. Morgado Chávez**[c] **and T. San José**[a]

[a]*Laboratoire de Physique des 2 Infinis Irène Joliot-Curie, CNRS/IN2P3, Université Paris-Saclay, 91405 Orsay Cedex, France*
[b]*Laboratoire de Physique Subatomique et de Cosmologie, CNRS/IN2P3, 38026 Grenoble Cedex, France*
[c]*Département de Physique Nucléaire, Irfu/CEA-Saclay, 91191 Gif-sur-Yvette Cedex, France*

E-mail: blossier@ijclab.in2p3.fr, mariane@lpsc.in2p3.fr, jose-manuel.morgadochavez@cea.fr, san-jose-perez@ijclab.in2p3.fr

Abstract: Distribution amplitudes are functions of non-perturbative matrix elements describing the hadronization of quarks and gluons. Thanks to factorization theorems, they can be used to compute the scattering amplitude of high-energy processes. Recently, new ideas have allowed their computation using lattice QCD, which should provide us with a general, fully relativistic determination. We present the first lattice calculation of the η_c-meson distribution amplitude at leading twist. Starting from the relevant matrix element in discrete Euclidean space on a set of $N_f = 2$ CLS ensembles, we explain the method to connect to continuum Minkowski spacetime. After addressing several sources of systematic uncertainty, we compare to Dyson-Schwinger and non-relativistic QCD determinations of this quantity. We find significant deviations between the latter and our result even at small Ioffe times.

Keywords: Hadronic Spectroscopy, Structure and Interactions, Lattice QCD, Parton Distributions

ArXiv ePrint: 2406.04668

https://doi.org/10.1007/JHEP09(2024)079

JHEP09(2024)079

Contents

1 Introduction

In 1964, Gell-Mann and Zweig postulated the existence of quarks as the underlying degrees of freedom in the eightfold way, the scheme to classify hadrons introduced back in 1961. Following their hypothesis, Taylor, Kendall and Friedman conducted a series of experiments in SLAC between 1966 and 1978, where they discovered the inner structure of hadrons. Their studies consisted of deep inelastic scattering (DIS) reactions probing protons and neutrons with electrons at high energies. Ever since, different inclusive and exclusive processes have been discovered to offer a privileged window to the structure of baryons and mesons. We focus in those exclusive scattering processes where there is a large momentum transfer to the hadron target and factorization theorems hold [1–3]. They allow to separate the amplitude in two main pieces: the scattering of the probe with quarks and gluons and the internal structure of the target. The first is calculable in perturbation theory and it is described by coefficient functions, while the second is a consequence of QCD confinement at low energies and it is given by a variety of soft distributions, like generalized parton distributions (GPDs) and distribution amplitudes (DAs). Examples of processes where the DA appears are meson photoproduction [4], $\gamma^*\gamma^* \to M$, and deeply virtual meson production (DVMP), in which an off-shell photon interacts with a target, a proton for example, and a meson is produced in the final state $\gamma^* p \to Mp$.

JHEP09(2024)079

The DA of a single meson, our object of interest, is a particular case of the more universal generalized distribution amplitudes (GDAs), which consider interacting hadrons, and depend on further degrees of freedom. GDAs and GPDs are connected via the crossing symmetry, allowing for a more uniform theoretical study of these quantities, see [5] for a review. Unfortunately, the non-perturbative nature of these functions makes them difficult to compute, and usually contribute the most to the cross-section uncertainty. In turn, this makes extracting information from experiments more difficult. Traditionally, the DA has been studied using non-relativistic QCD (NRQCD) [6, 7], Dyson-Schwinger (DS) equations [8–10], light-front dynamics [11] or light-cone sum rules [12, 13]. Of especial interest for our work are the studies of charmonium DAs employing the latter method in [14–17]. As these quantities are non-pertubative, it would be reasonable to think that lattice simulations are a natural choice to compute GPDs, DAs and other functions from first principles. Several works exist that reconstruct the DA from its first moments [18, 19]. However, it was not until 2013 that fundamental limitations were overcome in the seminal paper by Ji [20]. At the beginning, many efforts focused on the parton distribution function (PDF) of the nucleon [21, 22] and the PDF and DA of the pion and kaon [23–28], while other works aim now to compute their GPDs [29, 30] as well as the structure of heavy mesons [31]. See [32] for a review on the lattice progress. The latter are especially important to benefit the most from the EIC, EicC and LHC experiments, and with this project we aim at contributing to this effort. To this end, we present an *ab initio* calculation of the η_c-meson DA at leading twist, the first employing LQCD.

Let us start by defining the quantity of interest. The quark DA for a pseudoscalar state, which was introduced in 1977 [33] for the particular case of the pion, is given by the Fourier transform of a bi-local matrix element. In particular, using the light-cone metric in the light-cone gauge, $A^+ = 0$, the DA is given by [5]

$$\phi(x) = \int \frac{\mathrm{d}z^-}{2\pi} e^{-\mathrm{i}(x-1/2)p^+z^-} \left\langle \eta_c(p)|\bar{c}(-z/2)\gamma^+\gamma_5 c(z/2)|0\right\rangle \Big|_{z^+=z_\mathrm{T}=0}, \tag{1.1}$$

where $\langle\eta_c|$ is the pseudoscalar meson in the final state, $|0\rangle$ is the QCD vacuum, and c and $\bar{c}$ are the quark fields. The distance $z = (z^+, z^-, z_\mathrm{T})$, with $z^+ = z_\mathrm{T} = 0$, separates the quark fields and lies on the light-cone, $z^2 = 0$. Therefore, we may choose the direction p^+ for the η_c momentum. The definition in eq. (1.1) may include an additional i factor to match the definition of the pseudoscalar decay constant, all while having a real-valued function ϕ. However, this factor i simply redefines the phase of the meson state and it is not observable. Due to Lorentz invariance, this function depends solely on the plus-momentum fraction of the quark with respect to the meson, $x = q^+/p^+$. In other gauges, a straight Wilson line $W(-z^-/2, z^-/2)$ appears between the two field positions $-z^-/2$ and $z^-/2$ to ensure gauge invariance,

$$W(a,b) = P\exp\left(\mathrm{i}g\int_b^a \mathrm{d}z^-\, A^+(z^- n_-)\right) \tag{1.2}$$

where P indicates path ordering from a to b. Neither DAs, nor GPDs or other related functions can be computed using lattice simulations because, in Euclidean metric, only the null vector lies on the light cone. In [20], Ji proposed a generalization of PDFs to space-like separations, e.g. $z = (0, 0, z_3, 0)$ and $p = (0, 0, p_3, E)$ in Euclidean space, commonly known as quasi-PDFs, which tend towards the light-cone PDFs in the infinite momentum limit

JHEP09(2024)079

$p_3 \to \infty$. A similar approach can be applied to DAs and GPDs [34]. However, it was noted by Radyushkin in [35] that the dependence of quasi-PDFs on their momentum is rather complicated, and that $p_3 \geq 3\,\text{GeV}$ are necessary to approach their behavior at infinity. This requirement is still difficult to meet and, in particular, our set of ensembles have lattice spacings too coarse to reach the desired momentum.

In the same work [35], an alternative method was proposed, known as pseudo distributions, which are related via Fourier transform to Ioffe-time pseudo-distributions. The latter are given by bi-local matrix elements in terms of the Ioffe time $\nu = pz = p_3 z_3$ [36] and z_3^2. These pseudo distributions also generalize the light-cone distributions to spacelike intervals, and tend towards them in the short distance limit $z_3^2 \to 0$. The factor $1/z_3^2$ plays an analogous role to a renormalization scale μ^2. In our work, we employ the proposal in [35] as we understand the systematics are more favorable for our setup.

The remainder of this paper is organized as follows: in section 2, we define the fundamental object which is computed on the lattice, the reduced Ioffe-time pseudo-DA (rpITD), we explain how we extract it, how we model the light-cone DA (LCDA), and how we relate the two. In section 3, we detail our lattice calculation and the set of $N_f = 2$ ensembles that we use. In section 4, we take the continuum limit using three different lattice spacings. Since our ensembles include a variety of pion masses, we also take into account the subleading quark dependence. Finally, we present there the leading-twist DA of the η_c-meson, which is the main result of this work. Section 5 is devoted to estimate several sources of systematic uncertainties, while section 6 compares our results with alternative methods relying on NRQCD and DS equations. We give our conclusions in section 7.

2 Methodology

In Euclidean metric, we start from the matrix element [37]

$$M^\alpha(p,z) = e^{-ipz/2}\,\langle \eta_c(p)|\bar{c}(0)\gamma^\alpha\gamma_5 W(0,z)c(z)|0\rangle \tag{2.1}$$

where W is the $0 \to z$ straight Wilson line, $\langle\eta_c(p)|$ is the pseudoscalar meson state with momentum p, $|0\rangle$ is the QCD vacuum, $\bar{c}$ and c are quark fields, and the Wilson line W along the vector z ensures gauge invariance of the matrix element. Computing the matrix element in an asymmetric configuration as in eq. (2.1) allows to access all the lattice sites in the simulation, and to connect with the symmetric definition given in eq. (1.1), we use translation invariance and multiply by the appropriate phase, $\exp(-ipz/2)$. A Lorentz decomposition divides M^α in two pieces [37],

$$M^\alpha(p,z) = 2p^\alpha \mathcal{M}(p,z) + z^\alpha \mathcal{M}'(p,z) \tag{2.2}$$

where $\mathcal{M}$ carries both the leading-twist contribution and a higher-twist contamination at $\mathcal{O}\left(z^2\Lambda_{\text{QCD}}^2\right)$, while $\mathcal{M}'$ is a purely higher-twist effect. To remove $\mathcal{M}'$, we align the momentum along the z-axis, $p = (0,0,p_3,E)$, set an equal-time separation $z = (0,0,z_3,0)$ and select $\alpha = 4$, such that $M^4(p,z) = 2E\mathcal{M}(p,z)$. Note that $\mathcal{M}$ is a Lorentz invariant, and therefore it only depends on scalar combinations of p and z, which are ν and z^2. To take the continuum limit the operator $\bar{c}(0)\gamma^\alpha\gamma_5 W(0,z)c(z)$ needs to be renormalized, and while standard DAs $\phi(x,\mu)$ are

JHEP09(2024)079

defined in the $\overline{\text{MS}}$ scheme and exhibit a logarithmic dependence on the renormalization scale μ [5, 38], pseudo-DAs (pDAs) $\phi(x, z_3^2)$ have ultraviolet singularities and diverge logarithmically in the limit $z^2 \to 0$. To suppress the first, the authors of [37, 39, 40] use the results from [41], where it is proven that the entire operator is multiplicatively renormalizable. Since the renormalization constant only depends on z_3, we cancel it forming a renormalization group invariant (RGI) ratio that can be factorized using the $\overline{\text{MS}}$ scheme into the DA and Wilson coefficients. The result is the RGI ratio [37, 39, 40]

$$\tilde{\phi}(\nu, z) \equiv \frac{\mathcal{M}(p, z)\mathcal{M}(0, 0)}{\mathcal{M}(0, z)\mathcal{M}(p, 0)} \tag{2.3}$$

where $\nu = pz$ is the Ioffe time. The ratio $\tilde{\phi}(\nu, z)$ is a Lorentz scalar, and it depends solely on ν and z^2, but for notational convenience we suppress the square. We call eq. (2.3) the reduced Ioffe-time pseudo-DA (rpITD) from now on, and this is the actual quantity extracted from the lattice data. Let us briefly discuss the form of eq. (2.3). The factor $\mathcal{M}(0, z)$ cancels the renormalization factor of $\mathcal{M}(p, z)$, and it corresponds to a local axial-vector current in the limit $z = 0$. Said current should be conserved and normalized. However, this is not the case in lattice simulations due to lattice artifacts. To cancel the latter, we form the ratios $\mathcal{M}(p, z)/\mathcal{M}(p, 0)$ and $\mathcal{M}(0, z)/\mathcal{M}(0, 0)$, and then we divide the first by the second, cancelling the renormalization factors. This cancellation holds at all orders in perturbation theory [41], and the double ratio in eq. (2.3) has a well defined continuum limit and does not require an additional renormalization factor.

Regarding the logarithmic divergences in the limit $z^2 \to 0$, the matching relation eq. (2.4) cancels them. Specifically, upon removing the QFT regulator and any remaining higher-twist contamination (see section 4), we can relate the leading- twist rpITD $\tilde{\phi}_{\text{lt}}(\nu, z)$ and the light-cone Ioffe-time DA (ITD) $\tilde{\phi}_{\text{lt}}(\nu, \mu)$ in the $\overline{\text{MS}}$ scheme via the matching kernel C, which is derived in [34, 42] at next-to-leading order (NLO) in perturbation theory. Since the rpITD is RGI, its z^2 behavior is scheme-independent, but its dependence on this scale must match the μ dependence of the $\overline{\text{MS}}$ ITD. After performing the matching, we can Fourier-transform to obtain the LCDA at leading twist $\phi_{\text{lt}}(x, \mu)$,

$$\tilde{\phi}_{\text{lt}}(\nu, z) = \int_0^1 \mathrm{d}w\, C(w, \nu, z\mu) \int_0^1 \mathrm{d}x \cos(wx\nu - w\nu/2)\phi_{\text{lt}}(x, \mu), \tag{2.4}$$

where we choose the renormalization scale $\mu = 3\,\text{GeV}$ throughout this work. Inverting the Fourier transform in eq. (2.4) with only a limited number of data points in $\tilde{\phi}_{\text{lt}}(\nu, z)$ is an ill-posed problem which requires adding some extra information. In particular, we parametrize the DA $\phi_{\text{lt}}(x, \mu)$ in terms of the shifted Gegenbauer polynomials $\tilde{G}(x) \equiv G(-1 + 2x)$ [43, chapter 18], where $x \in [0, 1]$ and G are the standard ultraspherical polynomials defined in the domain $g \in [-1, 1]$. The left-hand side is determined thanks to the lattice simulations. Furthermore, we exchange the order of integration, expanding the cosine in a series of $\tilde{G}$ and computing the moments of C in powers of w.

Let us explain more in detail the procedure. Starting with the LCDA parameterization, at leading twist and leading order in α_s, the Gegenbauer polynomials $\tilde{G}^{(3/2)}(x)$ are eigenvectors of the Efremov-Radyushkin-Brodsky-Lepage (ERBL) equations describing the DA evolution [44].

JHEP09(2024)079

This means that, at this order, one can express the DA as a polynomial series with coefficient 3/2 [45, 46],

$$\phi_{\rm lt}(x,\mu) = 6x(1-x)\sum_{n=0}^{\infty} d_n^{(3/2)}(\mu)\tilde{G}_n^{(3/2)}(x). \tag{2.5}$$

The DA is then an analytic function normalized to one, $\int \mathrm{d}x\,\phi = 1$. In this project, we assume that eq. (2.5) is also a reasonable model of the DA that we compute non-perturbatively. If we were to use the infinite series of polynomials, the latter could describe functions like $1/x$ and $1/(1-x)$, and so the DA does not have to vanish at the endpoints $x = 0$ and $x = 1$. In practice, we truncate eq. (2.5) at small n, and the DA vanishes at the boundaries. Since the lattice data provides no information in this region, we are introducing some model dependence. After this discussion, we need to adapt eq. (2.5) to the particular case of charmonium, where the DA should be symmetric around $x = 1/2$. Since Gegenbauer polynomials with n odd are anti-symmetric, their corresponding coefficients vanish. Besides, we can leave the coefficient 3/2 undetermined and fit it to our data to speed up the convergence of the series. Changing the coefficient, which we call λ from now on, amounts to choosing one particular basis of polynomials, but it is always possible to transform back to eq. (2.5). Therefore, we will employ the following expression to describe the charmonium light-cone DA,

$$\phi_{\rm lt}(x,\mu) = (1-x)^{\lambda-1/2}x^{\lambda-1/2}\sum_{n=0}^{\infty} d_{2n}^{(\lambda)}\tilde{G}_{2n}^{(\lambda)}(x), \qquad d_0^{(\lambda)} = \frac{4^\lambda}{B\left(1/2,\lambda+1/2\right)} \tag{2.6}$$

where B is a beta function and the cofficients λ and d_{2n} will be constrained with our lattice data. Eq. (2.6) is normalized to one and we can recover eq. (2.5) replacing $\lambda = 3/2$. A similar approach has been used in the context of PDFs [22].

The next step is to compute the moments of the matching kernel C derived in [34, 42],

$$c_n(\nu, z\mu) = \int_0^1 \mathrm{d}w\, C(w,\nu,z\mu)w^n = 1 - \frac{\alpha_{\rm s}C_{\rm F}}{2\pi}\left[\log\left(\frac{\mu^2}{\mu_0^2}\right)b_n(\nu) + l_n(\nu)\right] \tag{2.7}$$

where $C_F = 4/3$ is the Casimir in the fundamental representation, $\mu = 3\,\mathrm{GeV}$, and the initial energy scale μ_0 is given by the Wilson line,

$$\frac{1}{\mu_0^2} \equiv \frac{z^2\, e^{2\gamma_{\rm E}+1}}{4} \tag{2.8}$$

where $\gamma_{\rm E}$ is the Euler constant. We use the strong coupling constant in the $\overline{\rm MS}$-scheme [47] $\alpha_s = 0.2243$, together with $\Lambda \equiv \Lambda^{(2)}_{\rm QCD} = 330\,\mathrm{MeV}$ [48] and $n_f = 2$ flavors. The functions b_n and l_n are given in terms of hypergeometric functions ${}_pF_q$,

$$\begin{aligned} b_n(\nu) = &-\frac{1}{2} - \sum_{j=0}^{n-1}\frac{2}{j+2}\,{}_1F_2\left(1,\frac{j+3}{2},\frac{j+4}{2},-\frac{\nu^2}{16}\right) - \frac{\nu^2}{24}\,{}_2F_3\left(1,1,2,2,\frac{5}{2},-\frac{\nu^2}{16}\right) \\ &+ \frac{1}{(n+2)(n+1)}\,{}_1F_2\left(1,\frac{n+3}{2},\frac{n+4}{2},-\frac{\nu^2}{16}\right) \end{aligned} \tag{2.9}$$

JHEP09(2024)079

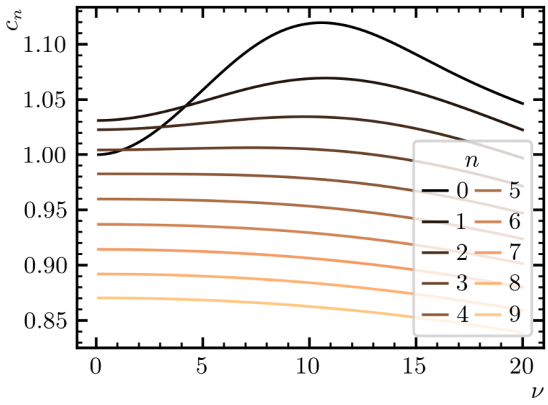

Figure 1. Moments $c_n(\nu, z_3\mu)$ of the DA matching kernel versus Ioffe time. For illustration, we set $z_3 = 5 \times 0.0658\,\text{fm}$.

and

$$l_n(\nu) = 1 + 4\sum_{j=0}^{n-1} \binom{n}{j+1} \frac{(-1)^j}{(j+1)^2}\, {}_2F_3\left(\frac{j+1}{2}, \frac{j+1}{2}, \frac{1}{2}, \frac{j+3}{2}, \frac{j+3}{2}, -\frac{\nu^2}{16}\right) + \frac{\nu^2}{8}\, {}_3F_4\left(1,1,1,\frac{3}{2},2,2,2,-\frac{\nu^2}{16}\right) - \frac{2}{(n+2)(n+1)}\, {}_1F_2\left(1,\frac{n+3}{2},\frac{n+4}{2},-\frac{\nu^2}{16}\right). \tag{2.10}$$

Note that all the hypergeometric functions ${}_pF_q$ in eqs. (2.9) and (2.10) fulfill $p \leq q$, which is sufficient to prove that they converge for all values of Ioffe time [49]. In figure 1, we plot c_n for several n's as a function of Ioffe time. In our analysis we will only use the lines for even n's.

Now we are in a position to rewrite the relation between the rpITD in the continuum and the light-cone DA, eq. (2.4). In essence, we expand the cosine in a Taylor series, separating the variables w, ν and x. Then, we perform the integral over w, which yields the moments of the matching kernel $c_{2k}(\nu, z\mu)$, and we expand the powers of $x - 1/2$ in terms of Gegenbauer polynomials. This procedure yields

$$\tilde{\phi}_{\text{lt}}(\nu, z) = \int_0^1 \mathrm{d}x\, K(x, \nu, z\mu)\phi_{\text{lt}}(x, \mu) \tag{2.11}$$

where the new kernel $K(x, \nu, z\mu)$ is an infinite series

$$K(x, \nu, z\mu) = \sum_{n=0}^{\infty} \frac{\sigma_{2n}^{(\lambda)}(\nu, z\mu)}{A_{2n}^{(\lambda)}} \tilde{G}_{2n}^{(\lambda)}(x). \tag{2.12}$$

The normalization of Gegenbauer polynomials is

$$A_n^{(\lambda)} = \frac{2^{1-2\lambda}\pi\Gamma(n+2\lambda)}{(n+\lambda)\Gamma(\lambda)^2 n!} \tag{2.13}$$

with the gamma functions Γ. The new set of functions σ_n are given by

$$\sigma_n^{(\lambda)}(\nu, z\mu) = \sum_{k=0}^{\infty} \left(-\frac{\nu^2}{4}\right)^k \frac{c_{2k}(\nu, z\mu)}{\Gamma(2k+1)} I(n, k, \lambda) \tag{2.14}$$

JHEP09(2024)079

where $c_{2k}(\nu, z\mu)$ are the moments of the matching kernel and $I(n,k,\lambda)$ is proportional to the Mellin transform of Gegenbauer polynomials,

$$I(n,k,\lambda) = \frac{2\pi}{4^{\lambda+k} n!} \frac{\Gamma(1+2k)\Gamma(n+2\lambda)}{\Gamma(\lambda)\Gamma\left(\lambda + \frac{n+2k+2}{2}\right)\Gamma\left(1+k-\frac{n}{2}\right)}. \tag{2.15}$$

The general expression of I simplifies to a beta function for the first values $n = 0, 2, 4, \ldots$ Finally, we use the DA parameterization eq. (2.6) such that the integral over x adopts the form of the orthogonality relation between Gegenbauer polynomials. As a consequence, eq. (2.4) can be rewritten as

$$\tilde{\phi}_{\rm lt}(\nu, z) = \sum_{n=0}^{\infty} \tilde{d}_{2n}^{(\lambda)} \sigma_{2n}^{(\lambda)}(\nu, z\mu), \qquad \tilde{d}_n^{(\lambda)} = \frac{d_n^{(\lambda)}}{4^\lambda}. \tag{2.16}$$

In section 4, we use eq. (2.16) to fit the coefficients d_{2n} and the parameter λ, which determine the LCDA, to the data obtained from the lattice after taking the continuum limit and removing the higher-twist effects. In the following, it is useful to define the leading order (LO) contribution to σ_n, which corresponds to the LO contribution to the matching kernel,

$$\sigma_{{\rm LO},n}^{(\lambda)}(\nu) = \sum_{k=0}^{\infty} \left(-\frac{\nu^2}{4}\right)^k \frac{I(n,k,\alpha)}{\Gamma(2k+1)} \tag{2.17}$$

as well as the NLO contribution,

$$\sigma_{{\rm NLO},n}^{(\lambda)} = \sigma_n^{(\lambda)} - \sigma_{{\rm LO},n}^{(\lambda)}. \tag{2.18}$$

In figure 2, we plot $\sigma_{{\rm LO},n}$ and $\sigma_{{\rm NLO},n}$ as a function of Ioffe time for several values of n. Note that all odd n's vanish. Looking at the LO contribution, which contributes the most to σ_n, we observe that each line peaks in a certain domain of Ioffe time and then vanishes. Given that we explore the range $\nu \lesssim 6$ in our calculation, we are most sensitive to σ_0 and its associated parameter d_0 and perhaps σ_2 and d_2, which peaks later. As we shall see, our data can only determine in practice λ and d_0, and we will set d_2, d_4, etc., to zero. Nonetheless, this will be sufficient to describe our lattice data.

3 Lattice setup

We employ the set of $N_f = 2$ Coordinated Lattice Simulations (CLS) ensembles collected in table 1. These data sets employ the Wilson plaquette gauge action and two mass-degenerate Wilson quarks with non-perturbative $\mathcal{O}(a)$-improvement. The pion masses range between $190\,\text{MeV} < m_\pi < 440\,\text{MeV}$, and κ_c is fixed so that $m_{D_S} = m_{D_S,\text{phys}} = 1968\,\text{MeV}$ [47]. The scale is set using f_K [50], which exhibits a milder mass extrapolation than the pion decay constant. For more details on the gauge simulations, see [50, 51] and references therein. We employ the package openQCD v2.0 [52] to compute the quark all-to-all propagators with wall sources diluted in spin. The Dirac equation is solved with deflated SAP-GCR [53–55], and the contractions are carried out with a custom version of the DD-HMC algorithm [56]. Throughout the analysis, statistical errors are propagated using the Gamma method detailed in [57–59]

JHEP09(2024)079

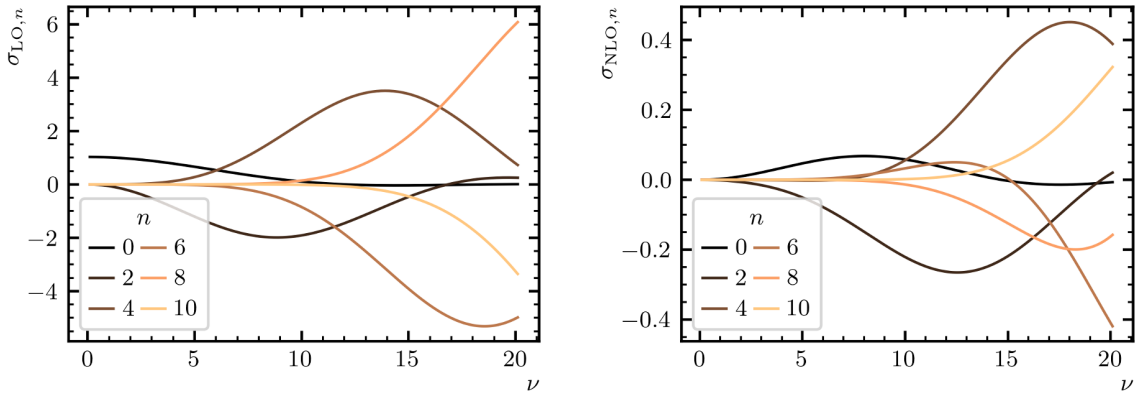

Figure 2. The LO contribution to σ_n, $\sigma_{\mathrm{LO},n}(\nu)$, and the NLO contribution, $\sigma_{\mathrm{NLO},n}(\nu, z\mu) = \sigma_n(\nu, z\mu) - \sigma_{\mathrm{LO},s}(\nu)$. We used $\lambda = 2.7$ and $z_3 = 5 \times 0.0658\,\mathrm{fm}$ as representative values.

id	β	a [fm]	L/a	am_π	m_π [MeV]	$m_\pi L$	κ_c	Measurements
A5	5.2	0.0755(9)(7)	32	0.1265(8)	331	4.0	0.12531	1980
B6			48	0.1073(7)	281	5.2	0.12529	1180
D5*	5.3	0.0658(7)(7)	24	0.1499(1)	449	3.6	0.12724	1500
E5			32	0.1458(3)	437	4.7	0.12724	2000
F6			48	0.1036(3)	311	5.0	0.12713	1200
F7			48	0.0885(3)	265	4.3	0.12713	2000
G8			64	0.0617(3)	185	4.1	0.12710	1790
N6	5.5	0.0486(4)(5)	48	0.0838(2)	340	4.0	0.13026	1900
O7			64	0.0660(1)	268	4.2	0.13022	1640

Table 1. The CLS ensembles used in this study. From left to right the ensemble label, the bare strong coupling, the lattice spacing [50], the number of lattice sites in every spatial direction ($T = 2L$), the approximate value of the pion mass [61], the proxy of finite-volume effects $m_\pi L$, the value of κ_c [62] and the number of measurements. Ensembles marked with an asterisk are only used to check the size of finite-size effects (FSEs) but are not included in the continuum extrapolation.

and implemented in [60]. The momentum p in the final-state meson is introduced using partially twisted boundary conditions (PTBC) [63] on one of the charm-quark fields, while the other retains anti-periodic boundary conditions (aPBC). Following the setup described in section 2 to isolate $\mathcal{M}$, we apply the twist angle θ in the z-direction, such that $p_3 L = \theta$ while $p_1 = p_2 = 0$. To obtain a realistic meson η_c and remove higher excitations, we form a Generalized Eigenvalue Problem (GEVP) with the interpolator $\bar{c}\gamma_5 c$ at four levels of Gaussian smearing [64], which correspond to the smearing radii $r/a = 0,\ 2.74,\ 3.54$ and 4.47. The links in the smearing operator employ ten iterations of APE smearing [65] to reduce their short distance fluctuations. To compute the DA we need the Wick contractions of M^α, which appear in figure 3. Looking at the disconnected piece first, it induces a mixing with the iso-singlet states η and η', but in our simulations the latter state cannot appear because the

JHEP09(2024)079

Figure 3. Wick contractions for the η_c meson. The double black vector represents a Wilson line and the red solid stripes show the charm-quark propagators. In this work, we only consider the quark-connected contribution on the left.

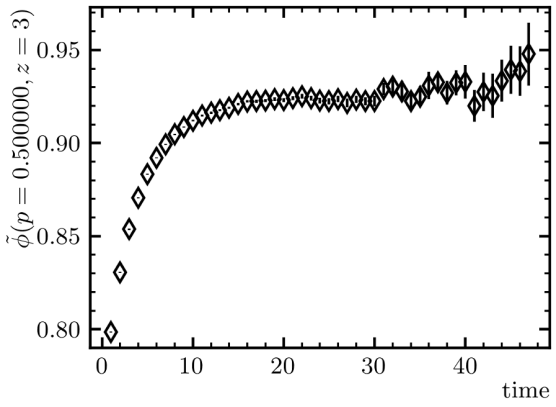

Figure 4. Double ratio in eq. (2.3) for parameters $ap = 0.5$ and $z_3/a = 3$ on ensemble F6. The rpITD $\tilde{\phi}(\nu, z)$ can be extracted from the plateau region between time slices 20 and 30.

strange-quark is quenched. We exclude this quark-disconnected contribution to simplify the analysis and because we expect it to be small due to Okubo-Zweig-Iizuka (OZI) suppression. In perturbation theory the diagram requires a two-gluon exchange, which means that it is suppressed by a factor $\alpha_s^2(\mu) \sim 0.05$ at our renormalization scale. A single gluon exchange vanishes because this is a vector state, and any expectation value where we project to a pseudoscalar state will vanish, requiring two gluons to obtain the correct quantum numbers.

The first step of the data analysis is forming eq. (2.1) and the RGI ratio eq. (2.3). At this stage, the latter shows some time dependence at early times due to excited states, see figure 4. They quickly decay leaving plateaus which are typically $\mathcal{O}(0.5\,\mathrm{fm})$ wide from where we can extract $\tilde{\phi}(\nu, z)$ fitting to a constant. However, one should not forget that all (ν, z^2) data on a given ensemble are correlated. Tackling the problem head-on, that is, fitting all plateaus in an ensemble simultaneously including their correlations is not possible, as the covariance matrix has a dimension of $\mathcal{O}(1000)$. Our statistics are not sufficient to properly estimate all entries and the matrix is not invertible. Instead, we exploit a hierarchy in the correlation matrix: data points (ν, z^2) at the same time slice are far more correlated than points at different time slices. This fact guides our approach to solve the problem. Instead of fitting to a plateau, we select a particular time slice to be $\tilde{\phi}(\nu, z)$ and carry out the entire analysis. This approach preserves the most important correlations in our data while providing a conservative error estimate. Of course, the choice of the time slice introduces a systematic that needs to be assessed (see section 5). The estimate of this uncertainty is the second error in table 2. After

JHEP09(2024)079

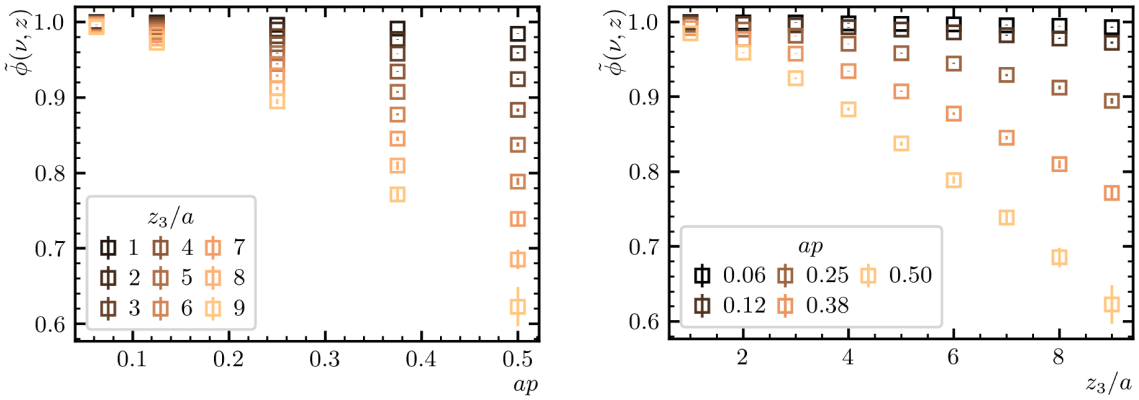

Figure 5. The rpITD defined in eq. (2.3) computed on ensemble G8 as a function of the final-state meson p and the extension of the Wilson line z_3/a.

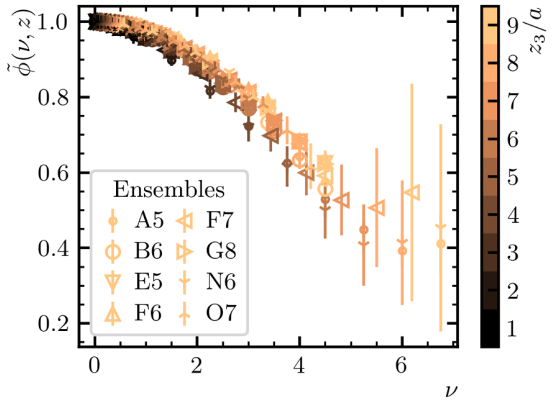

Figure 6. The rpITD as a function of Ioffe time on all the ensembles used in the continuum extrapolation. Different ensembles are shown with different markers, and different Wilson lines are given by the color gradient.

this step, we obtain the rpITD $\tilde{\phi}(\nu, z)$ as given by eq. (2.3). The result on ensemble G8 appears in figure 5 as a function of the final-state momentum p and the extension of the Wilson line. The complete data set, this time as a function of Ioffe time and the Wilson line, appears in figure 6. We notice that the data collapse to a nearly universal line, but important lattice artifacts remain which are accounted for in the continuum extrapolation.

4 Continuum limit

Once we have obtained $\tilde{\phi}(\nu, z)$ on every ensemble of table 1 at various Ioffe times ν and Wilson lines z, we remove the cutoff and match our results to the LCDA in one single step. See [22] for a study of PDFs using this approach. Although separating in two distinct steps the extrapolation and the problem with the inverse Fourier transform could be simpler, we would need several lattices for every momentum and Wilson line in physical units. See [66] for alternative methods to recover the DA from the ITD with only limited data. The first step to extrapolate to the continuum is building a model to account for the lattice artifacts,

JHEP09(2024)079

the higher-twist contamination, and the small quark mass dependence. We start by noting that the CP symmetry of the strong interactions constraints the behavior of the DA,

$$\tilde{\phi}(p,z) = \tilde{\phi}^*(-p,z) = \tilde{\phi}^*(p,-z) = \tilde{\phi}(-p,-z). \tag{4.1}$$

In particular, the equality $\tilde{\phi}(p,z) = \tilde{\phi}(-p,-z)$ restricts lattice artifacts with odd powers of a to be functions of $a|p|$ and $a/|z|$. Then, the lattice data $\tilde{\phi}(\nu,z)$ can be related to the continuum rpITD $\tilde{\phi}_{\rm con}(\nu,z)$ via a Taylor expansion in the lattice spacing,

$$\tilde{\phi}(\nu,z) = \tilde{\phi}_{\rm con}(\nu,z) + \sum_{r=1} \left(\frac{a}{|z|}\right)^r A_r(\nu) + (a\Lambda)^r\, B_r(\nu), \tag{4.2}$$

where we use $\Lambda \equiv \Lambda^{(2)}_{\rm QCD} = 330\,\text{MeV}$ [48] to render all terms dimensionless. Following [22], we introduce auxiliary functions A_r and B_r to model the Ioffe-time dependence of the lattice artifacts. We define them in analogous way to $\phi(x,\mu)$, and use the same basis of Gegenbauer polynomials,

$$\begin{aligned} A_r^{(\lambda)}(x) &= (1-x)^{\lambda-1/2} x^{\lambda-1/2} \sum_{s=0}^{S_{a,r}} a^{(\lambda)}_{r,2s} \tilde{G}^{(\lambda)}_{2s}(x), \\ B_r^{(\lambda)}(x) &= (1-x)^{\lambda-1/2} x^{\lambda-1/2} \sum_{s=0}^{S_{b,r}} b^{(\lambda)}_{r,2s} \tilde{G}^{(\lambda)}_{2s}(x). \end{aligned} \tag{4.3}$$

The unknown functional dependence is contained in the fit parameters $a_{r,2s}$ and $b_{r,2s}$. The function A_r in Ioffe time can be obtained via

$$A_r^{(\lambda)}(\nu) = \int_0^1 \mathrm{d}x\, A_r^{(\lambda)}(x) \cos\left(x\nu - \nu/2\right) = \sum_{s=0}^{S_{A,r}} \tilde{a}^{(\lambda)}_{r,2s} \sigma^{(\lambda)}_{\text{LO},2s}(\nu), \tag{4.4}$$

where $\tilde{a}_{r,2s} = a_{r,2s}/4^\lambda$. A similar result holds for B_r. Note that the integrand of $\sigma_{\text{LO},s}$ is even (odd) in the domain of integration for s even (odd), and only the even terms are non-zero. Finally, we set $a_{r,0} = 0$ because $\tilde{\phi}(\nu=0,z) = 1$. The continuum limit $\tilde{\phi}_{\rm con}$ is a sum of the leading-twist contribution in eq. (2.16) and higher-twist contamination. We emphasize that the latter piece includes the so-called target-mass corrections, which depend on the physical η_c-meson mass as $z^2 m^2_{\eta_c,\text{phy}}$. We model all higher-twist corrections using another auxiliary function, $C_r(\nu)$, which is analogous to A_r and B_r,

$$\tilde{\phi}(\nu,z) = \tilde{\phi}_{\rm lt}(\nu,z) + \sum_{n=1} \left(\frac{a}{|z|}\right)^n A_n(\nu) + (a\Lambda)^n B_n(\nu) + (z^2\Lambda^2)^n C_n(\nu). \tag{4.5}$$

Note that the target-mass effects are absorbed in the definition of the $C_r(\nu)$ fit parameters. Since we remove them before matching to the light-cone, we need not modify the kernel $C(w,\nu,z\mu)$ to take the meson mass into account. As the only effect of the light-quark on the DA comes from the fermionic determinant, we may expect a polynomial expansion in the light-quark mass m_ℓ, which has itself a chiral expansion in m_π^2 at LO. We checked that the latter function is enough to describe the pion mass dependence for ensembles at $\beta = 5.3$. Besides, we take into account the small mistuning in the charm-quark mass with another

JHEP09(2024)079

term proportional to the η_c mass, m_{η_c}, which we obtain from the GEVP. After trying several functional combinations, we observe that the type of model which describes best our data is

$$\begin{aligned}\tilde{\phi}(\nu,z) = \tilde{\phi}_{\rm lt}(\nu,z) + \sum_{n=1}\Bigg[&\left(\frac{a}{|z|}\right)^n A_n(\nu) + (a\Lambda)^n B_n(\nu) + (z^2\Lambda^2)^n C_n(\nu) \\ &+ \left(\frac{a}{|z|}\right)^n \left(\Lambda^{-1}\left(m_{\eta_c} - m_{\eta_c,\rm phy}\right) D_n(\nu) + \Lambda^{-2}\left(m_\pi^2 - m_{\pi,\rm phy}^2\right) E_n(\nu)\right)\Bigg],\end{aligned} \tag{4.6}$$

where we normalize by the physical masses [47]

$$m_{\eta_c,\rm phy} = 2983.9(4)\,\text{MeV}, \quad m_{\pi,\rm phy} = 134.9768(5)\,\text{MeV} \tag{4.7}$$

and we have introduced further auxiliary functions $D(\nu)$ and $E(\nu)$ with the same form as $A(\nu)$. In practice, our data is only sensitive to the first coefficient $n = 1$ in the series of auxiliary functions, the first nonzero coefficient for each function $A(\nu)$, $B(\nu)$, etc., and the first term in $\tilde{\phi}_{\rm lt}(\nu,z)$, so that our model simplifies to

$$\begin{aligned}\tilde{\phi}(\nu,z) = \tilde{\phi}_{\rm lt}(\nu,z) + &\frac{a}{|z|}A_1(\nu) + a\Lambda B_1(\nu) + z^2\Lambda^2 C_1(\nu) \\ &+ \frac{a}{|z|}\Big(\Lambda^{-1}\left(m_{\eta_c} - m_{\eta_c,\rm phy}\right) D_1(\nu) + \Lambda^{-2}\left(m_\pi^2 - m_{\pi,\rm phy}^2\right) E_1(\nu)\Big).\end{aligned} \tag{4.8}$$

To fit eq. (4.8) to our lattice data we minimize a chi-square using the variable projection (VP) algorithm —see [67] for the original work, and appendix A for our particular implementation. We include the correlations among the data on each ensemble, and tame very small eigenvalues in the covariance matrix using the averaging method outlined in [68] and implemented in [60]. We find the minimum at $\chi^2/\text{dof} = 368/467 = 0.79$ and the results are gathered in table 2. Looking at its second column, where the fit parameter estimates appear, we observe that λ lies far away from its asymptotic value of 1.5. Furthermore, we observe a certain hierarchy in the coefficients: those associated with terms proportional to $a/|z|$ and the mistuning of the charm-quark mass are the most relevant, followed by pure lattice artifacts, the pion mass dependence and higher-twist effects. Nonetheless, every term is necessary to describe the data well, and in particular we observe non-zero higher-twist effects, which include target-mass corrections. See section 5 for an explanation of the two systematic errors. Now we can evaluate the LCDA defined in eq. (2.6) using the first term in the series and $\lambda = 2.73(18)$,

$$\phi_{\rm lt}(x,\mu) = \frac{4^\lambda (1-x)^{\lambda-1/2} x^{\lambda-1/2}}{B\left(1/2, 1/2+\lambda\right)}, \tag{4.9}$$

where we used the fact that $\tilde{G}_0(x) = 1$. The plot of $\phi(x,\mu)$ can be seen in figure 7. We tried to add higher coefficients to describe the DA, in particular d_2 and d_4, which correspond to $\tilde{G}_2(x)$ and $\tilde{G}_4$, respectively. Although they are both compatible with zero, our data has not sufficient range in ν to determine them reliably.

5 Systematics

Lattice simulations are performed in a finite volume, but it is only after estimating the infinite volume limit that we can compare our results to physical quantities. The associated difference

JHEP09(2024)079

λ	$2.73 \pm 0.12 \pm 0.12 \pm 0.06$	2.75(12)	2.61(15)	2.62(10)
$a_{1,2}$	$-7.58 \pm 0.05 \pm 0.59 \pm 0.55$	−8.12(5)	−8.68(13)	−6.76(4)
$b_{1,2}$	$0.88 \pm 0.07 \pm 0.08 \pm 0.06$	0.89(7)	0.77(10)	0.81(7)
$c_{1,2}$	$-0.042 \pm 0.002 \pm 0.005 \pm 0.001$	−0.0428(22)	−0.0440(28)	−0.0407(24)
$d_{1,2}$	$-2.221 \pm 0.015 \pm 0.063 \pm 0.15$	−2.368(15)	−2.52(4)	−2.000(11)
$e_{1,2}$	$-0.0897 \pm 0.001 \pm 0.159 \pm 0.116$	−0.1700(16)	−0.321(5)	−0.068 48(12)

Table 2. Expected value and uncertainty for each fit parameter. The first column labels the parameter. The second column corresponds to a global fit to all table 1 ensembles except D5. The first uncertainty in this column indicates the statistical error, the second shows the variation of our result depending on the time slice selected as $\tilde{\phi}(\nu, z)$ (see section 3), and the third the extrapolation uncertainty. The third column removes the heavier pion mass, E5, from the fit, and the fourth column includes only ensembles with $m_\pi < 300\,\text{MeV}$. In the fifth column, we remove all Wilson lines with $z_3/a > 0.5\,\text{fm}$. For details about the systematic errors and this table, see section 5.

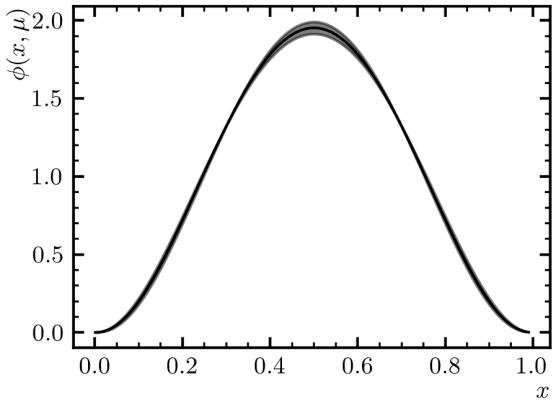

Figure 7. The LCDA of the η_c-meson. The band shows the statistical error.

between the two results, or FSEs, are especially difficult to estimate in the case of concern here, a non-local matrix element. Some works have explored this problem, and for example the authors of [69] give analytic expressions for a non-local matrix element with scalar currents. Although it omits the Wilson line, one can see that the main FSEs stem from the pion as a decreasing exponential of $m_\pi L$, plus some extra function for the η_c in terms of $m_{\eta_c}(L - z)$. Their subsequent work in [70] determines the same quantity non-perturbatively in terms of the form factors of the asymptotic hadron state. Yet, the estimation of FSEs for non-local matrix elements remains a complicated subject, and no theoretical prediction exists for the DA. Several studies of the nucleon PDFs report negligible effects [21, 71], while other detect them with some significance [72]. In the case of the pion PDF, the authors of [23] perform a fit to capture the volume effects directly. In our calculation, we compare the results for the rpITD $\tilde{\phi}(\nu, z)$ on ensembles D5 and E5, which only differ by their volume, and found very good agreement. Therefore, we neglect FSEs in our project and do not attempt to correct our data.

As already mentioned in section 3, an important source of systematic uncertainty originates in the extraction of $\tilde{\phi}(\nu, z)$ from the lattice data. The ratio in eq. (2.3) shows a

JHEP09(2024)079

residual time dependence, although a wide plateau is visible for all the momenta and Wilson lines. For a given ensemble, we choose one time slice as the rpITD $\tilde{\phi}(\nu, z)$ (the same for all (ν, z^2)) and extrapolate to the continuum. In this way we can keep the correlations between the different Ioffe times and Wilson lines intact, all while the correlation matrix remains invertible. Accounting for all the possible time slices that can be chosen on the various ensembles, there are more than 3.5 million possible extrapolations to the continuum. To estimate the impact of our choice on the final result, we sample nearly 16000 cases. The spread of the results, which is Gaussian, gives the second uncertainty in table 2.

To further test the stability of the continuum extrapolation we perform two cuts in the pion mass. First, we fit only ensembles with $m_\pi < 400\,\text{MeV}$, which removes ensemble E5. Second, we perform a more stringent cut and we only fit $m_\pi < 300\,\text{MeV}$, which further removes A5, F6 and N6. The result of both fits appear in table 2 together with the fit that considers all ensembles. We observe that the physical parameter λ remains compatible while some of the nuisance parameters have a more pronounced shift, especially $e_{1,2}$ that takes care of the pion-mass dependence. We employ the mass cuts to estimate the systematic uncertainty associated to the extrapolation, which is fixed to half the distance between the fit to all ensembles and the cut furthest away. This is the third uncertainty in table 2.

The perturbative matching we use in section 2 is only valid for sufficiently short Wilson lines. In particular, [73] argues that $z_3 \leq 0.5\,\text{fm}$ is necessary. In our analysis, see for instance figure 6, five Wilson lines exceed this mark: $z_3/a > 6$ for $\beta = 5.2$ and $z_3/a > 7$ for $\beta = 5.3$. To test the validity of our results, we repeat the extrapolation to the continuum as given in section 4, which also includes the matching procedure, removing these Wilson lines. The result we obtain with this reduced data set is $\lambda = 2.62(10)$, $\chi^2/\text{dof} = 388/374 = 1.04$. The uncertainty is slightly smaller since the data with the largest z^2 are noisier than average. We report the value of all parameters in this fit on the fifth column of table 2. The value of λ is compatible with our preferred result (see second column of table 2), and we use this as a corroboration of our analysis. We decide against adding the difference between the two results as an extra systematic uncertainty, and we rather see the proximity of both as proof that, in our case, it is safe to include slightly longer Wilson lines. Regarding the nuisance parameters, the situation is similar, with the variation well explained by our predetermined error budget. In particular, the value of $c_{1,2}$, which controls the size of higher-twist corrections, is unchanged within errors.

Before finishing this section, we note several other systematic uncertainties that we cannot estimate at the moment. Most important of all, the strange quark is quenched, and its effects on our determination can only be estimated reliably including it in the action. Second, an extra lattice spacing would allow us to estimate the $\mathcal{O}(a^2)$ dependence neglected in our continuum extrapolation. Finally, we consider the pion mass dependence in our results, and although it is only a subleading effect, having an ensemble at the physical pion mass would remove any systematic associated with the extrapolation in the mass.

6 Comparison to other approaches

As a last step, we compare our *ab initio* determination of the DA to the NRQCD calculation in [7] and the DS method used in [8]. The former alternative assumes that the charm-quarks

JHEP09(2024)079

	This work	DS	NRQCD
$\langle g^2 \rangle$	0.134(6)	0.118(18)	0.171(23)
$\langle g^4 \rangle$	0.043(4)	0.036(9)	0.018 808(19)

Table 3. First nonzero moments of the DA as determined by this work, by the DS approach in [8], and by the NRQCD calculation in [7]. We define $g = -1 + 2x$ for $x \in [0, 1]$.

can be approximated as non-relativistic particles, whose DA at LO is a Dirac delta centered at $x = 1/2$. The authors of [7] further include the first relativistic and quantum corrections, which they note are of the same size, to produce a more accurate description. In appendix C, we gather the important equations for this method. The latter alternative [8] solves the DS equations to obtain Bethe-Salpeter wave functions [74, 75], which are related to the DA. The data on the light cone are subsequently fitted to a finite-width representation of a Dirac delta, which appears together with the other important parameters of this method in appendix D. To compare to the latter, we also need to evolve the DA in [8] from their original scale, $\tilde{\mu} = 2\,\text{GeV}$, to ours, $\mu = 3\,\text{GeV}$. To solve the evolution equations we employ the APFEL++ suite [76, 77].

Especially for NRQCD, it is interesting to Fourier-transform to Ioffe-time space and compare the various determinations, getting rid of the Dirac delta and its derivatives appearing in x space. The Fourier transform of the NRQCD and DS DAs appears in appendices C and D, while the Fourier transform of our DA is simply given by

$$\tilde{\phi}_{\text{lt}}(\nu, \mu) = \sum_{n=0}^{\infty} \tilde{d}_{2n} \sigma_{\text{LO},2n}(\nu). \tag{6.1}$$

The three DAs appear in figure 8, and we observe excellent agreement between the lattice and the DS determination, while both show a very different behavior from NRQCD for larger Ioffe times. The band estimates the uncertainty of each determination: for our result, it is the total error; for NRQCD, it is the uncertainty of $\langle v^2 \rangle$, a parameter defined in appendix C; and for DS, it indicates the deviation between the data points obtained from the DS equations and the functional form used to fit them. Furthermore, observe that at leading order the NRQCD DA is equal to 1, and the first-order corrections are just as large around $\nu \sim 6$, with the quantum loops and the relativistic correction of similar size. Therefore, we argue that one should extend the NRQCD calculation to the next order in both quantum and relativistic corrections.

Finally, we compute the first Mellin moments for each determination,

$$\langle g^n \rangle (\mu) = \int_0^1 \mathrm{d}x\, g^n \phi(x, \mu), \tag{6.2}$$

where $g = -1 + 2x$ and only even n's are non-zero. Appendices B–D gather the expressions for the moments, and we show $\langle g^2 \rangle$ and $\langle g^4 \rangle$ in table 3. Once more, we find good agreement only with the DS method. Looking at the Mellin moments of NRQCD in appendix C, we see that $\langle v^2 \rangle$ only contributes for $\langle g^2 \rangle$, and further corrections should be included to estimate $\langle g^4 \rangle$. This explains the tiny uncertainty in $\langle g^4 \rangle$.

7 Conclusions

We present the first lattice calculation of the η_c-meson DA, which is parametrized in eq. (4.9). We compute the pseudo-DA on the lattice and match it to the light-cone DA, which we

JHEP09(2024)079

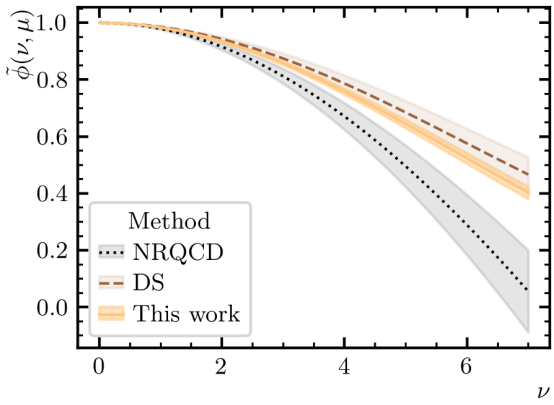

Figure 8. Comparison in Ioffe-time space between the DA as determined in this work, by NRQCD [7] and by DS [8]. The bands reflect the uncertainties reported on each work, ours indicating the total error.

study via a series of Gegenbauer polynomials that allows for systematic improvement upon extending the data to larger Ioffe times. We employ three different lattice spacings and a wide range of pion masses, allowing us to take the continuum limit accounting for the subleading effects of the quark masses. We study several systematics, and in particular we find that FSEs are negligible. We compare our results in the continuum to other approaches, and find good agreement with the Dyson-Schwinger equations, while we strongly disagree with the NRQCD prediction at all but the smallest Ioffe times. In the future we will address several sources of systematics with a new set of simulations at the physical pion mass which include also the strange and charm quarks in the sea.

Acknowledgments

The work by J.M. Morgado Chávez has been supported by P2IO LabEx (ANR-10-LABX-0038) in the framework of Investissements d'Avenir (ANR-11-IDEX-0003-01). The work by T. San José is supported by Agence Nationale de la Recherche under the contract ANR-17-CE31-0019. This project was granted access to the HPC resources of TGCC (2021-A0100502271, 2022-A0120502271 and 2023-A0140502271) by GENCI. The authors thank Michael Fucilla, Cédric Mezrag, Lech Szymanowski, and Samuel Wallon for valuable discussions.

A Variable projection

All but one fit parameters in eq. (4.8) are linear. This suggests that we should separate the extrapolation to the continuum limit in a nonlinear minimization, where only λ is optimized, and a linear minimization, where all the linear fit parameters are obtained from the optimal value of λ. This idea is commonly known as variable projection (VP), it was originally suggested in [67], and implementations for different types of problems exist in Python [78], Matlab [79] and other languages. See [80] for a review of the general concept and applications.

JHEP09(2024)079

In this section, we present our implementation. Start from the common chi-square

$$\chi_1^2 = (\bar{y} - \eta)^T C^{-1} (\bar{y} - \eta) \tag{A.1}$$

where the column vector $\bar{y} \in \mathbb{R}^{n\times 1}$ contains the data, $\eta \in \mathbb{R}^{n\times 1}$ is the model, and $C \in \mathbb{R}^{n\times n}$ is the covariance matrix. For example, if we were fitting ensembles B6, F7 and O7, the data vector would be

$$\bar{y} = \left(\tilde{\phi}_{\mathrm{B6},0},\, \dots\, \tilde{\phi}_{\mathrm{B6},N_{\mathrm{B6}}-1},\, \tilde{\phi}_{\mathrm{F7},0},\, \dots\, \tilde{\phi}_{\mathrm{F7},N_{\mathrm{F7}}-1},\, \tilde{\phi}_{\mathrm{O7},0},\, \dots\, \tilde{\phi}_{\mathrm{O7},N_{\mathrm{O7}}-1}\right)^T, \tag{A.2}$$

where the dots run over all datapoints $\tilde{\phi}$ for a particular ensemble and $n = N_{\mathrm{B6}} + N_{\mathrm{F7}} + N_{\mathrm{O7}}$. In the same fashion, the covariance matrix would be block diagonal,

$$C = C_{\mathrm{B6}} \oplus C_{\mathrm{F7}} \oplus C_{\mathrm{O7}}, \tag{A.3}$$

and the chi-square χ_1^2 fits each data point $\bar{y}_i$ for $i = 0, \dots, n-1$ using the model

$$\eta_i = \sum_{j=0}^{q-1} \mathfrak{q}_j \Phi_{i,j}(\mathfrak{r}) + \Theta_i(\mathfrak{r}) \tag{A.4}$$

which has q linear fit parameters $\mathfrak{q} \in \mathbb{R}^{q\times 1}$ and r nonlinear fit parameters $\mathfrak{r} \in \mathcal{S}_{\mathfrak{r}} \subset \mathbb{R}^{r\times 1}$, all organized in column vectors. $\mathcal{S}_{\mathfrak{r}}$ is the subspace of values that the parameters $\mathfrak{r}$ are allowed to adopt given the physical constraints of the problem. $\Phi(\mathfrak{r}) \in \mathbb{R}^{n\times q}$ is a matrix of nonlinear functions of $\mathfrak{r}$, which is a mapping between the latter and a linear transformation $\mathcal{L}(\mathbb{R}^n, \mathbb{R}^q)$. $\Theta_i(\mathfrak{r})$ is a column vector of similar properties to $\Phi(\mathfrak{r})$. Using the extrapolation model eq. (4.8) as an example, $\mathfrak{r}$ has only one entry,

$$\mathfrak{r} = \left(\lambda\right). \tag{A.5}$$

If we expand $\tilde{\phi}_{\mathrm{lt}}$ up to $n = 4$ and we include several nuisance functions with only one parameter, the linear fit parameters are

$$\mathfrak{q} = \left(d_2,\, d_4,\, a_{1,2},\, b_{1,2},\, c_{1,2}\right)^T \tag{A.6}$$

and the columns of Φ and Θ contain the information about

$$\Phi_i = \left(\sigma_2,\, \sigma_4,\, \frac{a}{|z|}\sigma_{\mathrm{LO},2},\, a\Lambda\sigma_{\mathrm{LO},2},\, z^2\Lambda^2\sigma_{\mathrm{LO},2}\right), \quad \Theta_i = \left(\frac{4^\lambda \sigma_0}{B(1/2, \lambda + 1/2)}\right) \tag{A.7}$$

where each row evaluates a given point (ν, z). We suppose the minimum chi-square is obtained for certain values $(\hat{\mathfrak{r}}, \hat{\mathfrak{q}})$,

$$\min_{\mathfrak{r},\mathfrak{q}} \chi_1^2 = \chi_1^2(\hat{\mathfrak{r}}, \hat{\mathfrak{q}}). \tag{A.8}$$

When building the covariance matrix C, we control its small eigenvalues using the averaging procedure given in [68]. Then, we can decompose the covariance matrix, $C^{-1} = (L^{-1})^T L^{-1}$, define new variables

$$A \equiv L^{-1}\Phi \in \mathbb{R}^{n\times q}, \qquad B \equiv L^{-1}\Theta \in \mathbb{R}^{n\times 1}, \qquad y \equiv L^{-1}\left(\bar{y} - \Theta\right) \in \mathbb{R}^{n\times 1}, \tag{A.9}$$

JHEP09(2024)079

and rewrite the chi-square problem as a 2-norm,

$$\chi_1^2 = \|y - A\mathfrak{q}\|_2^2. \tag{A.10}$$

Rewriting our problem in the form of eq. (A.10) enables us to use the results of [67], although we must take into account that y is also a function of the nonlinear parameters $\mathfrak{r}$. For a given value of $\mathfrak{r}$, the minimum of χ_1^2 occurs at

$$\hat{\mathfrak{q}} = A^+ y, \tag{A.11}$$

where the generalized left inverse of A is given by

$$A^+ = \left(A^T A\right)^{-1} A^T. \tag{A.12}$$

The form of A^+ is problematic because we need to compute the inverse of a large $n \times n$ matrix which can be singular or almost singular. Fortunately, we may choose other definitions for A^+ because the property it needs to fulfill is $AA^+A = A$. To improve stability, we choose the singular value decomposition (SVD)

$$A = USV^\dagger \to A^+ = VS^{-1}U^\dagger, \tag{A.13}$$

where U and V are unitary matrices, and S is a diagonal matrix containing the singular values of A. In our case, A is real and has not full rank, and so $U \in \mathbb{R}^{n\times q}$, $S \in \mathbb{R}^{q\times q}$, and $V \in \mathbb{R}^{q\times q}$. Just as in [67], we can obtain the optimal parameters $\hat{\mathfrak{r}}, \hat{\mathfrak{q}}$ with the following algorithm:

1. Obtain the optimal values $\hat{\mathfrak{r}}$ minimizing the modified norm

$$\chi_2^2(\mathfrak{r}) = \left\|P^\perp y\right\|_2^2, \quad P^\perp = 1 - AA^+. \tag{A.14}$$

2. Obtain the optimal fit parameters $\hat{\mathfrak{q}}$ using

$$\hat{\mathfrak{q}} = A^+(\hat{\mathfrak{r}})y(\hat{\mathfrak{r}}). \tag{A.15}$$

3. The fit quality is given by

$$\min_{\mathfrak{r},\mathfrak{q}} \chi_1^2 = \chi_1^2(\hat{\mathfrak{r}}, \hat{\mathfrak{q}}) = \min_{\mathfrak{r}} \chi_2^2 = \chi_2^2(\hat{\mathfrak{r}}). \tag{A.16}$$

For the minimization of χ_2^2 we need its gradient with respect to $\mathfrak{r}$, which is given by [67]

$$\nabla\chi_2^2(\lambda) = y^T \nabla P^\perp y + 2y^T P^\perp \nabla y. \tag{A.17}$$

The last term does not appear in [67] because they do not consider the possibility of an affine fit function Θ. The derivative of the projector is

$$\nabla P^\perp = -\left(P^\perp \nabla A A^+ + \left(P^\perp \nabla A A^+\right)^T\right) \tag{A.18}$$

while the derivative of the shifted datapoints is simply

$$\nabla y = -L^{-1}\nabla\Theta. \tag{A.19}$$

JHEP09(2024)079

B Moments of the DA

The Mellin moments of the parameterization in eq. (2.6) are

$$\langle g^n \rangle = \begin{cases} 0 & \text{if n is odd,} \\ \dfrac{1}{4^\lambda} \sum_{j=0}^{\lfloor n/2 \rfloor} d_{2j}^{(\lambda)} I\left(2j, \frac{n}{2}, \lambda\right) & \text{if n is zero or even,} \end{cases} \tag{B.1}$$

where I is defined in eq. (2.15), and $n = 0, 1, 2, \ldots$, $2j = 0, 1, 2, \ldots, n$, and $\lambda > -1/2$ but $\lambda \neq 0$. Using our result $\lambda = 2.73(18)$ and neglecting the parameters $d_2 = d_4 = \cdots = 0$, the first couple of nonzero DA moments are

$$\left\langle g^2 \right\rangle = \frac{I(1,0,\lambda)}{B\left(\frac{1}{2}, \frac{1}{2}+\lambda\right)} = 0.134(6), \qquad \left\langle g^4 \right\rangle = \frac{I(2,0,\lambda)}{B\left(\frac{1}{2}, \frac{1}{2}+\lambda\right)} = 0.043(4). \tag{B.2}$$

We are making a clear systematic error in the determination of the moments, since we are not able to measure d_2, d_4, etc. However, the method is systematically improvable as we extend the domain of data to larger Ioffe times.

The moments $\langle g^n \rangle$ and the Gegenbauer moments $d_n^{(3/2)}$ are related by

$$\langle g^n \rangle = A_n + \sum_{j=1}^{n} d_n^{(3/2)} B_{n,j} \tag{B.3}$$

where

$$A_n = \begin{cases} 0 & \text{if n is odd,} \\ \dfrac{3}{2}\left(\dfrac{1}{1+n} - \dfrac{1}{3+n}\right) & \text{if n is even or zero,} \end{cases} \tag{B.4}$$

and

$$B_{n,j} = \begin{cases} \dfrac{3}{2^{n+3}} \dfrac{\sqrt{\pi}(j+2)(j+1)n!}{\Gamma\left(\frac{5}{2} + \frac{n+j}{2}\right)\Gamma\left(1 + \frac{n-j}{2}\right)} & \text{if } n+j \text{ is even and } j \leq n, \\ 0 & \text{otherwise} \end{cases} \tag{B.5}$$

The first few nonzero values of the coefficients A_n and $B_{n,j}$ appear in table 4, and the first nonzero Gegenbauer moments are

$$d_2^{(3/2)} = \frac{7}{12}\left(5\langle g^2 \rangle - 1\right) = -0.192(19), \qquad d_4^{(3/2)} = \frac{77}{8}\langle g^4 \rangle - \frac{77}{12}\langle g^2 \rangle + \frac{11}{24} = 0.007(6). \tag{B.6}$$

C NRQCD approach

In this appendix, we gather the equations used to compute the NRQCD prediction of the DA, which is given in x-space as (see [7] and references therein)

$$\phi(x,\mu) = \phi^{(0)}(x) + \frac{\alpha_s(\mu) C_F}{4\pi}\phi^{(1)}(x) + \langle v^2 \rangle \phi^{(v^2)}(x) + \mathcal{O}\left(\alpha_s^2, \alpha_s v, v^4\right). \tag{C.1}$$

JHEP09(2024)079

n	0	2	4	6		
A_n	1	1/5	3/35	1/21		
n	1	2	3	3	4	4
j	1	2	1	3	2	4
$B_{n,j}$	3/5	12/35	9/35	4/21	8/35	8/77

Table 4. First nonzero coefficients A_n and $B_{n,j}$ used to relate the moments $\langle g^n \rangle$ and the Gegenbauer moments $d_n^{(3/2)}$ of the DA.

The parameter $\langle v^2 \rangle = 0.222(70)$ [7] is the relativistic correction to the long-distance matrix element (LDME). The other functions are given by [81–83]

$$\begin{aligned}
\phi^{(0)}(x) &= \delta(x-1/2),\\
\phi^{(1)}(x) &= \left(\log\frac{\mu_0^2}{m_Q^2}-1\right)\left[4x\frac{1+2\bar{x}}{1-2x}\theta(1-2x)\right]_{++} - \left[8x\frac{1+2\bar{x}}{1-2x}\log(1-2x)\theta(1-2x)\right]_{++}\\
&\quad + \left[\frac{16x\bar{x}}{(1-2x)^2}\theta(1-2x)\right]_{+++} + \Delta\left[16x\theta(1-2x)\right]_{++} + (x\longleftrightarrow\bar{x}),\\
\phi^{(v^2)}(x) &= \frac{1}{24}\delta^{(2)}\left(x-\frac{1}{2}\right).
\end{aligned} \tag{C.2}$$

The plus prescriptions are given by

$$\begin{aligned}
\int_0^1 \mathrm{d}x\,[f(x)]_{++}g(x) &= \int_0^1 \mathrm{d}x\,f(x)(g(x)-g(1/2)),\\
\int_0^1 \mathrm{d}x\,[f(x)]_{+++}g(x) &= \int_0^1 \mathrm{d}x\,f(x)(g(x)-g(1/2)-g'(1/2)(x-1/2)),
\end{aligned} \tag{C.3}$$

for generic functions $f(x)$ and $g(x)$, and the ITD of eq. (C.1) is

$$\tilde{\phi}(\nu,\mu) = 1 + \frac{\alpha_s(\mu)C_F}{4\pi}\left(\left[\log\left[\frac{\mu_0^2}{m_Q^2}\right]-1\right]A(\nu)+B(\nu)+C(\nu)+\Delta D(\nu)\right) - \langle v^2\rangle\frac{\nu^2}{24}, \tag{C.4}$$

where the quantum corrections are

$$\begin{aligned}
A(\nu) &= 4\,\mathrm{Ci}\left(\frac{\nu}{2}\right) - 4\log\left(\frac{\nu}{2}\right) - 4\gamma - \frac{8}{\nu}\sin\left(\frac{\nu}{2}\right) + 3 + \frac{8}{\nu^2}\left(1-\cos\left(\frac{\nu}{2}\right)\right),\\
B(\nu) &= \frac{\nu^2}{4}{}_3\mathrm{F}_4\left(1,1,1,\frac{3}{2},2,2,2,-\frac{\nu^2}{16}\right) - 4{}_2\mathrm{F}_3\left(\frac{1}{2},\frac{1}{2},\frac{1}{2},\frac{3}{2},\frac{3}{2},-\frac{\nu^2}{16}\right)\\
&\quad - {}_2\mathrm{F}_3\left(1,1,\frac{1}{2},2,2,-\frac{\nu^2}{16}\right) + 5,\\
C(\nu) &= 8 - 4\cos\left(\frac{\nu}{2}\right) - \frac{8}{\nu}\sin\left(\frac{\nu}{2}\right) - 2\nu\,\mathrm{Si}\left(\frac{\nu}{2}\right),\\
D(\nu) &= 4 + \frac{32}{\nu^2}\left(1-\cos\left(\frac{\nu}{2}\right)\right).
\end{aligned} \tag{C.5}$$

Ci and Si are the cosine and sine integrals and ${}_pF_q$ are hypergeometric functions. Since $p \le q$, their convergence is guaranteed for all Ioffe times [49]. The parenthesis multiplying α_s

JHEP09(2024)079

vanishes at $\nu = 0$, such that $\tilde{\phi}(\nu = 0, \mu) = 1$. To plot the DA we need several parameters: we take the typical energy scale for the NRQCD LDME, μ_0, to be $2\bar{m}_c$, the $\overline{\text{MS}}$ charm-quark mass $\bar{m}_c = 1.27(2)\,\text{GeV}$ [47], and we take the one-loop corrected $\overline{\text{MS}}$ mass for a given quark [84]

$$m_c = \bar{m}_c \left(1 + \frac{1}{\pi}\alpha(\bar{m}_c)C_F\right) = 1.46(2)\,\text{GeV}. \tag{C.6}$$

The even Mellin moments of eq. (C.1) are given by

$$\begin{aligned}\left\langle g^{2n}\right\rangle = \frac{\langle v^2\rangle}{3}\delta_{n,1} + \frac{\alpha_s(\mu)C_F}{2\pi}\Bigg\{&\left[\log\left(\frac{\mu_0^2}{m_Q^2}\right) - 1\right]\left(\frac{1}{n} - \frac{1}{2n+1} - \frac{1}{2n+2}\right)\\ &+ \frac{1}{n^2} - \frac{2}{(2n+1)^2} - \frac{1}{2(1+n)^2} + \frac{2}{2n-1} - \frac{2}{2n+1}\\ &+ 4\Delta\left(\frac{1}{2n+1} - \frac{1}{2n+2}\right)\Bigg\}.\end{aligned} \tag{C.7}$$

D Dyson-Schwinger approach

In this section, we gather the equations used in the DS approach to compute the DA. The authors of [8] propose to model the DA like a finite-width representation of the static limit, $\delta(x - 1/2)$. That is, they propose a function that is convex-concave-convex in the range $x \in [0, 1]$,

$$\phi(g) = \frac{3}{2}N_\lambda(1 - g^2)e^{-(\lambda g)^2} \tag{D.1}$$

where $\lambda = 1.70(27)$. Denoting the error function by erf, the normalization is

$$N_\lambda^{-1} = \frac{1}{8\lambda^3}\left(3(2\lambda^2 - 1)\sqrt{\pi}\,\text{erf}(\lambda) + 6\lambda e^{-\lambda^2}\right). \tag{D.2}$$

The ITD corresponding to eq. (D.1) is

$$\begin{aligned}\phi(\nu, \mu) = \frac{3}{4\lambda}N_\lambda\Bigg[&\sqrt{\pi}\left(1 - \frac{1}{2\lambda^2} + \frac{\nu^2}{16\lambda^4}\right)\exp\left(-\frac{\nu^2}{16\lambda^2}\right)\Re\,\text{erf}\left(\lambda - \frac{\nu\text{i}}{4\lambda}\right)\\ &+ \left(\frac{1}{\lambda}\cos\left(\frac{\nu}{2}\right) - \frac{\nu}{4\lambda^3}\sin\left(\frac{\nu}{2}\right)\right)e^{-\lambda^2}\Bigg].\end{aligned} \tag{D.3}$$

The even moments of eq. (D.1) are

$$\left\langle g^{2n}\right\rangle = \frac{3}{4}\frac{N_\lambda}{\lambda^{2n+1}}\left[\gamma\left(n + 1/2, \lambda^2\right) - \frac{1}{\lambda^2}\gamma\left(n + 3/2, \lambda^2\right)\right] \tag{D.4}$$

where γ is the lower incomplete gamma function. The odd moments are zero, while $\langle 1\rangle = 1$ so that the DA is normalized.

JHEP09(2024)079

References

[1] J.C. Collins, D.E. Soper and G.F. Sterman, *Factorization of Hard Processes in QCD*, *Adv. Ser. Direct. High Energy Phys.* **5** (1989) 1 [hep-ph/0409313] [INSPIRE].

[2] A.V. Radyushkin, *Asymmetric gluon distributions and hard diffractive electroproduction*, *Phys. Lett. B* **385** (1996) 333 [hep-ph/9605431] [INSPIRE].

[3] J.C. Collins, L. Frankfurt and M. Strikman, *Factorization for hard exclusive electroproduction of mesons in QCD*, *Phys. Rev. D* **56** (1997) 2982 [hep-ph/9611433] [INSPIRE].

[4] G.P. Lepage and S.J. Brodsky, *Exclusive Processes in Perturbative Quantum Chromodynamics*, *Phys. Rev. D* **22** (1980) 2157 [INSPIRE].

[5] M. Diehl, *Generalized parton distributions*, *Phys. Rept.* **388** (2003) 41 [hep-ph/0307382] [INSPIRE].

[6] G.T. Bodwin, E. Braaten and G.P. Lepage, *Rigorous QCD analysis of inclusive annihilation and production of heavy quarkonium*, *Phys. Rev. D* **51** (1995) 1125 [*Erratum ibid.* **55** (1997) 5853] [hep-ph/9407339] [INSPIRE].

[7] H.S. Chung et al., *Pseudoscalar Quarkonium+γ Production at NLL+NLO accuracy*, *JHEP* **10** (2019) 162 [arXiv:1906.03275] [INSPIRE].

[8] M. Ding et al., *Leading-twist parton distribution amplitudes of S-wave heavy-quarkonia*, *Phys. Lett. B* **753** (2016) 330 [arXiv:1511.04943] [INSPIRE].

[9] D. Binosi et al., *Distribution Amplitudes of Heavy-Light Mesons*, *Phys. Lett. B* **790** (2019) 257 [arXiv:1812.05112] [INSPIRE].

[10] F.E. Serna et al., *Distribution amplitudes of heavy mesons and quarkonia on the light front*, *Eur. Phys. J. C* **80** (2020) 955 [arXiv:2008.09619] [INSPIRE].

[11] A.J. Arifi, L. Happ, S. Ohno and M. Oka, *Structure of heavy mesons in the light-front quark model*, *Phys. Rev. D* **110** (2024) 014020 [arXiv:2401.07933] [INSPIRE].

[12] V.M. Braun, *Light cone sum rules*, in the proceedings of the *4th International Workshop on Progress in Heavy Quark Physics*, Rostock, Germany, September 20–22 (1997) [hep-ph/9801222] [INSPIRE].

[13] V.M. Braun et al., *Moments of pseudoscalar meson distribution amplitudes from the lattice*, *Phys. Rev. D* **74** (2006) 074501 [hep-lat/0606012] [INSPIRE].

[14] V.V. Braguta, A.K. Likhoded and A.V. Luchinsky, *The study of leading twist light cone wave function of eta(c) meson*, *Phys. Lett. B* **646** (2007) 80 [hep-ph/0611021] [INSPIRE].

[15] V.V. Braguta, *The study of leading twist light cone wave functions of J/psi meson*, *Phys. Rev. D* **75** (2007) 094016 [hep-ph/0701234] [INSPIRE].

[16] V.V. Braguta, *The study of leading twist light cone wave functions of 2S state charmonium mesons*, *Phys. Rev. D* **77** (2008) 034026 [arXiv:0709.3885] [INSPIRE].

[17] V.V. Braguta, A.K. Likhoded and A.V. Luchinsky, *Leading twist distribution amplitudes of P-wave nonrelativistic mesons*, *Phys. Rev. D* **79** (2009) 074004 [arXiv:0810.3607] [INSPIRE].

[18] RQCD collaboration, *Light-cone distribution amplitudes of pseudoscalar mesons from lattice QCD*, *JHEP* **08** (2019) 065 [*Addendum ibid.* **11** (2020) 037] [arXiv:1903.08038] [INSPIRE].

[19] RQCD collaboration, *Light-cone distribution amplitudes of octet baryons from lattice QCD*, *Eur. Phys. J. A* **55** (2019) 116 [arXiv:1903.12590] [INSPIRE].

JHEP09(2024)079

[20] X. Ji, *Parton Physics on a Euclidean Lattice*, *Phys. Rev. Lett.* **110** (2013) 262002 [arXiv:1305.1539] [INSPIRE].

[21] C. Alexandrou et al., *Systematic uncertainties in parton distribution functions from lattice QCD simulations at the physical point*, *Phys. Rev. D* **99** (2019) 114504 [arXiv:1902.00587] [INSPIRE].

[22] HADSTRUC collaboration, *The continuum and leading twist limits of parton distribution functions in lattice QCD*, *JHEP* **11** (2021) 024 [arXiv:2105.13313] [INSPIRE].

[23] B. Joó et al., *Pion valence structure from Ioffe-time parton pseudodistribution functions*, *Phys. Rev. D* **100** (2019) 114512 [arXiv:1909.08517] [INSPIRE].

[24] X. Gao et al., *Pion distribution amplitude at the physical point using the leading-twist expansion of the quasi-distribution-amplitude matrix element*, *Phys. Rev. D* **106** (2022) 074505 [arXiv:2206.04084] [INSPIRE].

[25] LATTICE PARTON collaboration, *Pion and Kaon Distribution Amplitudes from Lattice QCD*, *Phys. Rev. Lett.* **129** (2022) 132001 [arXiv:2201.09173] [INSPIRE].

[26] E. Baker et al., *Lattice QCD calculation of the pion distribution amplitude with domain wall fermions at physical pion mass*, *JHEP* **07** (2024) 211 [arXiv:2405.20120] [INSPIRE].

[27] HADSTRUC collaboration, *Extracting the Pion Distribution Amplitude from Lattice QCD through Pseudo-Distributions*, *PoS* **LATTICE2023** (2024) 300 [arXiv:2401.06858] [INSPIRE].

[28] J. Holligan and H.-W. Lin, *Pion valence quark distribution at physical pion mass of $N_f = 2 + 1 + 1$ lattice QCD*, *J. Phys. G* **51** (2024) 065101 [arXiv:2404.14525] [INSPIRE].

[29] S. Bhattacharya et al., *Generalized parton distributions from the pseudo-distribution approach on the lattice*, arXiv:2405.04414 [INSPIRE].

[30] HADSTRUC collaboration, *Towards unpolarized GPDs from pseudo-distributions*, *JHEP* **08** (2024) 162 [arXiv:2405.10304] [INSPIRE].

[31] S. Zhao and A.V. Radyushkin, *B-meson Ioffe-time distribution amplitude at short distances*, *Phys. Rev. D* **103** (2021) 054022 [arXiv:2006.05663] [INSPIRE].

[32] M. Constantinou, *The x-dependence of hadronic parton distributions: A review on the progress of lattice QCD*, *Eur. Phys. J. A* **57** (2021) 77 [arXiv:2010.02445] [INSPIRE].

[33] A.V. Radyushkin, *Deep Elastic Processes of Composite Particles in Field Theory and Asymptotic Freedom*, hep-ph/0410276 [INSPIRE].

[34] A.V. Radyushkin, *Generalized parton distributions and pseudodistributions*, *Phys. Rev. D* **100** (2019) 116011 [arXiv:1909.08474] [INSPIRE].

[35] A.V. Radyushkin, *Quasi-parton distribution functions, momentum distributions, and pseudo-parton distribution functions*, *Phys. Rev. D* **96** (2017) 034025 [arXiv:1705.01488] [INSPIRE].

[36] B.L. Ioffe, *Space-time picture of photon and neutrino scattering and electroproduction cross-section asymptotics*, *Phys. Lett. B* **30** (1969) 123 [INSPIRE].

[37] A. Radyushkin, *Nonperturbative Evolution of Parton Quasi-Distributions*, *Phys. Lett. B* **767** (2017) 314 [arXiv:1612.05170] [INSPIRE].

[38] A.V. Belitsky and A.V. Radyushkin, *Unraveling hadron structure with generalized parton distributions*, *Phys. Rept.* **418** (2005) 1 [hep-ph/0504030] [INSPIRE].

[39] K. Orginos, A. Radyushkin, J. Karpie and S. Zafeiropoulos, *Lattice QCD exploration of parton pseudo-distribution functions*, *Phys. Rev. D* **96** (2017) 094503 [arXiv:1706.05373] [INSPIRE].

JHEP09(2024)079

[40] J. Karpie, K. Orginos and S. Zafeiropoulos, *Moments of Ioffe time parton distribution functions from non-local matrix elements*, *JHEP* **11** (2018) 178 [arXiv:1807.10933] [INSPIRE].

[41] T. Ishikawa, Y.-Q. Ma, J.-W. Qiu and S. Yoshida, *Renormalizability of quasiparton distribution functions*, *Phys. Rev. D* **96** (2017) 094019 [arXiv:1707.03107] [INSPIRE].

[42] A.V. Radyushkin, *Quark pseudodistributions at short distances*, *Phys. Lett. B* **781** (2018) 433 [arXiv:1710.08813] [INSPIRE].

[43] *NIST Digital Library of Mathematical Functions*, https://dlmf.nist.gov/ [Release 1.1.10 of 2023-06-15].

[44] V.M. Braun, G.P. Korchemsky and D. Müller, *The uses of conformal symmetry in QCD*, *Prog. Part. Nucl. Phys.* **51** (2003) 311 [hep-ph/0306057] [INSPIRE].

[45] A.V. Efremov and A.V. Radyushkin, *Factorization and Asymptotical Behavior of Pion Form-Factor in QCD*, *Phys. Lett. B* **94** (1980) 245 [INSPIRE].

[46] G.P. Lepage and S.J. Brodsky, *Exclusive Processes in Quantum Chromodynamics: Evolution Equations for Hadronic Wave Functions and the Form-Factors of Mesons*, *Phys. Lett. B* **87** (1979) 359 [INSPIRE].

[47] Particle Data Group collaboration, *Review of Particle Physics*, *PTEP* **2022** (2022) 083C01 [INSPIRE].

[48] Flavour Lattice Averaging Group (FLAG) collaboration, *FLAG Review 2021*, *Eur. Phys. J. C* **82** (2022) 869 [arXiv:2111.09849] [INSPIRE].

[49] *Chapter III Hypergeometric Functions*, in *The Special Functions and Their Approximations*, Y.L. Luke ed., Elsevier (1969), p. 38–114 [DOI:10.1016/s0076-5392(08)62627-2].

[50] P. Fritzsch et al., *The strange quark mass and Lambda parameter of two flavor QCD*, *Nucl. Phys. B* **865** (2012) 397 [arXiv:1205.5380] [INSPIRE].

[51] J. Heitger, G.M. von Hippel, S. Schaefer and F. Virotta, *Charm quark mass and D-meson decay constants from two-flavour lattice QCD*, *PoS* **LATTICE2013** (2014) 475 [arXiv:1312.7693] [INSPIRE].

[52] M. Luscher and A. Schafer, *OpenQCD: Simulation programs for lattice QCD*.

[53] M. Luscher, *Solution of the Dirac equation in lattice QCD using a domain decomposition method*, *Comput. Phys. Commun.* **156** (2004) 209 [hep-lat/0310048] [INSPIRE].

[54] M. Luscher, *Deflation acceleration of lattice QCD simulations*, *JHEP* **12** (2007) 011 [arXiv:0710.5417] [INSPIRE].

[55] M. Luscher, *Local coherence and deflation of the low quark modes in lattice QCD*, *JHEP* **07** (2007) 081 [arXiv:0706.2298] [INSPIRE].

[56] M. Luscher and A. Scafer, *DD-HMC: Simulation program for two-flavour lattice QCD*.

[57] ALPHA collaboration, *Monte Carlo errors with less errors*, *Comput. Phys. Commun.* **156** (2004) 143 [*Erratum ibid.* **176** (2007) 383] [hep-lat/0306017] [INSPIRE].

[58] ALPHA collaboration, *Critical slowing down and error analysis in lattice QCD simulations*, *Nucl. Phys. B* **845** (2011) 93 [arXiv:1009.5228] [INSPIRE].

[59] A. Ramos, *Automatic differentiation for error analysis of Monte Carlo data*, *Comput. Phys. Commun.* **238** (2019) 19 [arXiv:1809.01289] [INSPIRE].

JHEP09(2024)079

[60] F. Joswig, S. Kuberski, J.T. Kuhlmann and J. Neuendorf, *pyerrors: A python framework for error analysis of Monte Carlo data*, *Comput. Phys. Commun.* **288** (2023) 108750 [arXiv:2209.14371] [INSPIRE].

[61] M. Della Morte et al., *The hadronic vacuum polarization contribution to the muon $g-2$ from lattice QCD*, *JHEP* **10** (2017) 020 [arXiv:1705.01775] [INSPIRE].

[62] R. Balasubramamian and B. Blossier, *Decay constant of B_s and B_s^* mesons from $N_f = 2$ lattice QCD*, *Eur. Phys. J. C* **80** (2020) 412 [arXiv:1912.09937] [INSPIRE].

[63] C.T. Sachrajda and G. Villadoro, *Twisted boundary conditions in lattice simulations*, *Phys. Lett. B* **609** (2005) 73 [hep-lat/0411033] [INSPIRE].

[64] S. Gusken, *A study of smearing techniques for hadron correlation functions*, *Nucl. Phys. B Proc. Suppl.* **17** (1990) 361 [INSPIRE].

[65] APE collaboration, *Glueball Masses and String Tension in Lattice QCD*, *Phys. Lett. B* **192** (1987) 163 [INSPIRE].

[66] J. Karpie, K. Orginos, A. Rothkopf and S. Zafeiropoulos, *Reconstructing parton distribution functions from Ioffe time data: from Bayesian methods to Neural Networks*, *JHEP* **04** (2019) 057 [arXiv:1901.05408] [INSPIRE].

[67] G.H. Golub and V. Pereyra, *The Differentiation of Pseudo-Inverses and Nonlinear Least Squares Problems Whose Variables Separate*, *SIAM J. Numer. Anal.* **10** (1973) 413.

[68] C. Michael and A. McKerrell, *Fitting correlated hadron mass spectrum data*, *Phys. Rev. D* **51** (1995) 3745 [hep-lat/9412087] [INSPIRE].

[69] R.A. Briceño, J.V. Guerrero, M.T. Hansen and C.J. Monahan, *Finite-volume effects due to spatially nonlocal operators*, *Phys. Rev. D* **98** (2018) 014511 [arXiv:1805.01034] [INSPIRE].

[70] R.A. Briceño and C.J. Monahan, *A model-independent framework for determining finite-volume effects of spatially nonlocal operators*, *Phys. Rev. D* **103** (2021) 094521 [arXiv:2102.01814] [INSPIRE].

[71] H.-W. Lin and R. Zhang, *Lattice finite-volume dependence of the nucleon parton distributions*, *Phys. Rev. D* **100** (2019) 074502 [INSPIRE].

[72] B. Joó et al., *Parton Distribution Functions from Ioffe time pseudo-distributions*, *JHEP* **12** (2019) 081 [arXiv:1908.09771] [INSPIRE].

[73] A.V. Radyushkin, *Theory and applications of parton pseudodistributions*, *Int. J. Mod. Phys. A* **35** (2020) 2030002 [arXiv:1912.04244] [INSPIRE].

[74] L. Chang et al., *Imaging dynamical chiral symmetry breaking: pion wave function on the light front*, *Phys. Rev. Lett.* **110** (2013) 132001 [arXiv:1301.0324] [INSPIRE].

[75] F. Gao et al., *Parton distribution amplitudes of light vector mesons*, *Phys. Rev. D* **90** (2014) 014011 [arXiv:1405.0289] [INSPIRE].

[76] V. Bertone, S. Carrazza and J. Rojo, *APFEL: A PDF Evolution Library with QED corrections*, *Comput. Phys. Commun.* **185** (2014) 1647 [arXiv:1310.1394] [INSPIRE].

[77] V. Bertone, *APFEL++: A new PDF evolution library in C++*, *PoS* **DIS2017** (2018) 201 [arXiv:1708.00911] [INSPIRE].

[78] A. Bärligea, P. Hochstaffl and F. Schreier, *A Generalized Variable Projection Algorithm for Least Squares Problems in Atmospheric Remote Sensing*, *Mathematics* **11** (2023) 2839.

JHEP09(2024)079

[79] D.P. O'Leary and B.W. Rust, *Variable projection for nonlinear least squares problems*, *Comput. Optim. Appl.* **54** (2012) 579.

[80] G. Golub and V. Pereyra, *Separable nonlinear least squares: the variable projection method and its applications*, *Inverse Prob.* **19** (2003) R1.

[81] X.-P. Wang and D. Yang, *The leading twist light-cone distribution amplitudes for the S-wave and P-wave quarkonia and their applications in single quarkonium exclusive productions*, *JHEP* **06** (2014) 121 [arXiv:1401.0122] [INSPIRE].

[82] G.T. Bodwin et al., *Relativistic corrections to Higgs boson decays to quarkonia*, *Phys. Rev. D* **90** (2014) 113010 [arXiv:1407.6695] [INSPIRE].

[83] W. Wang, J. Xu, D. Yang and S. Zhao, *Relativistic corrections to light-cone distribution amplitudes of S-wave B_c mesons and heavy quarkonia*, *JHEP* **12** (2017) 012 [arXiv:1706.06241] [INSPIRE].

[84] R. Tarrach, *The Pole Mass in Perturbative QCD*, *Nucl. Phys. B* **183** (1981) 384 [INSPIRE].

JHEP09(2024)079